Study of elastic properties of polymers from microhardness tests

R. Rikards*, F. J. Baltá Calleja**, A. Flores**,
D. R. Rueda**, and V. Kushnevski*

*Institute of Computer Analysis of Structures, Riga Technical University, Kalku St. 1, LV-1658, Riga, Latvia

**Instituto de Estructura de la Materia, CSIC, Serrano 119, Madrid, 28006, Spain

ABSTRACT

A numerical method of identification to derive the elastic properties of polymers from indentation experiments has been developed. Five different polymers were tested: amorphous and semi-crystalline polyethylene terephtalate (PET), semi-crystalline polyvinylidene fluoride (PVF_2), a copolymer of polyvinylidene fluoride and trifluorethylene, $P(VF_2/F_3E)$ 60/40, and high pressure crystallised polyethylene (PE). The elastic properties of the polymers are calculated by two methods. On the basis of finite element solution, a simple function relating the load to the indentation depth and elastic modulus is first obtained. The elastic properties are then derived from the load-indentation depth experimental data (loading curve). A second method to determine the elastic properties is based on using the experimental data of the unloading curve. Elastic properties obtained from loading and unloading curves are in good agreement.

1. INTRODUCTION

While the use of the polymer and fibre reinforced polymer materials was rapidly growing in the last years, it became apparent that the classical techniques for measuring the material properties did no longer satisfy the needs [1]. Many problems arose, due to the microscopically heterogeneous character and the high degree of anisotropy in these materials. Simultaneously due to the evolution of computer science, numerical techniques for solving problems in solid mechanics became more and more widespread [1]. During the last decade investigations to develop a new technique for material identification, the so-called mixed numerical-experimental technique, started [2].

Mixed numerical-experimental methods are the subject of model errors because the numerical model is always based on a series of hypotheses. If the real structure does not satisfy one or more of these hypotheses, the model of the structure is evidently not appropriate. Since the development of mixed numerical-experimental techniques for material identification is aimed at obtaining a practical method which yields quick and reliable results, a lot of research has been done in order to minimise these model errors [1-4]. In the meantime many different approaches were produced for identification of the physical parameters directly characterising structural behaviour (i.e. Young's modulus and density of the material). Bolognini et. al. [3] used the appropriate comparison between actual eigenfrequencies of an existing structure and eigenfrequencies obtained via finite element analysis. It led to the identification of parameters which can be used for the calibration of the model as well as for the detection of a damaged zones in the structure. Numerical-experimental identification methods mainly are used in structural applications. For example, Mota Soares [4] identified the elastic properties of laminated composites by using the experimental eigenfrequencies.

Contact problems were analysed by many investigators [5-7]. Friction at the contact surfaces, elastoplastic behaviour of the material and other non-linearities can be taken into account by using numerical methods: the finite element method or the boundary element one. Finite element solutions of indentation problems have been obtained by Bhattacharrya and Nix [8], Giannakopouluos et al. [9] and other investigators.

In the present investigation the mixed numerical-experimental technique is used to determine the elastic properties of polymers. The experimental data obtained from microhardness tests have been employed to identify the plane strain elastic modulus $E^*=E/(1-\nu^2)$, where E is Young's modulus and ν the Poisson's ratio. As numerical experimental data, the results of finite element solution of the contact problem have been used. The data obtained by the finite element analysis are used to determine a simple function relating the load with the indentation depth and the plane strain elastic modulus. The finite element solution is obtained by using a finite element program ANSYS [10]. In the present investigation the pyramidal (Vickers) indenter is approximated by an axisymmetric cone [11].

Conventional microhardness testers use diamond indenters which penetrate the surface of a sample upon application of a given load at a constant rate [12]. The diagonal length of the residual impression is optically measured immediately after the removal of the diamond to minimize the viscoelastic effects. The microhardness is proportional by some geometrical constant to the ratio of the applied load to the square of the diagonal length of the impression. The permanent plastic deformation of the indented surface has been shown to provide information about the morphology and microstructure of polymers [12]. However, the information concerning the immediate elastic recovery of the sample is lost. In the present paper we have used an ultra-microhardness tester technique, where the penetration depth of

the indentation is instantly computer-recorded as a function of the applied load and subsequent removal of it. This technique, thus, opens up the possibility of investigating the elastic properties of the material.

2. EXPERIMENTAL

2.1 Materials

Five different polymers were tested: amorphous and semi-crystalline polyethylene terephtalate (PET), semi-crystalline polyvinylidene fluoride (PVF_2), the 60/40 copolymer of polyvinylidene fluoride and trifluorethylene $P(VF_2/F_3E)$ and high crystallinity polyethylene (PE) crystallised at high pressure. The samples of poly(ethylene teraphtalate) (PET) supplied by Prof. Zachmann (University of Hamburg) were melt pressed to about 200 μm thick films and quenched in ice-water. The amorphous films were finally isothermally annealed at 150^{0}C for 1h giving rise to semi-crystalline materials (crystallinity: 35%) [13]. Commercial pellets of PVF_2 and $P(VF_2/F_3E)$ 60/40 from Atochem were also pressure moulded to about 200 μm thick films, and the films were subsequently quenched in ice water [14]. Crystallinity of the copolymer $P(VF_2/F_3E)$ 60/40 is about 75% [14], and that of PVF_2 is about 50% [15]. The high molecular weight sample of PE (Hifax) was supplied by Prof. Basset (University of Reading). This sample was crystallised at 260^{0}C under a pressure of 500 MPa [16]. The thickness of the PE sample was 2 mm.

2.2 Techniques

In the present investigation the experiments were performed in a Shimadzu dynamic ultra microhardness tester in conjunction with a Vickers indenter. Indentations were separated by at

least 50 μm. The following relation between units for the force is used: 1 gf=0.1 mN. Other units are presented in the SI system. The minimum load that can be applied is 0.01 gf with a precision of 1%. The displacement of the indenter is recorded with a precision of 10^{-3} μm. Cycles of the type load-hold-unload were performed (see Fig. 1). In all cases, the maximum load applied was of 15.1 gf, which is of the same order of magnitude of the contact loads used in conventional microhardness tests [12]. Typical indentation depths corresponding to a 15.1 gf load are about 6-6.5 μm for amorphous PET. The load-unloading rate was 1.35 gf/s. The maximum applied load was held for six seconds. For series of amorphous PET the maximum load applied was also held for 100 seconds (8 experiments) to check out the viscoelastic response of the material. All experiments were performed at room temperature (~20° C).

Data corresponding to each load-hold-unload cycle were transferred to a computer program for their analysis. Each load-hold-unload cycle is defined by approximately 600 points. Typical load-unloading curves for different polymers are shown in Fig. 2a-e. It is seen that for PE (Fig. 2e) and P(VF_2/F_3E) (Fig. 2d) there are significant plastic deformations while for amorphous (Fig. 2a) and semi-crystalline PET (Fig. 2b) rather low values of plastic deformations are obtained. It is noteworthy that high pressure crystallized PE shows the highest elastic stiffness.

2.3 Analysis of indentation

The elastic response of the material can be determined using the experimental *P-h* data from the loading and unloading curves. From this plot, the elastic, viscoelastic and plastic contributions to the indentation depth, *h*, can be separated. In Fig. 3, a typical experimental

plot of h versus time t for amorphous PET is presented showing the loading and unloading cycles. The elastic h_e, plastic h_p and viscoelastic h_v deformations can now be separated according to the expression:

$$h = h_e + h_p + h_v \tag{1}$$

For a typical amorphous PET specimen, for which h vs. t diagram is presented in Fig. 3, the full indentation depth is h=6.62 μm, the elastic part is h_e=2.39 μm, the viscoelastic part is h_v=0.6 μm and plastic part is h_p=3.63 μm. It is seen that the plastic deformation is about 55% of the total deformation, while the elastic deformation is 36% and the viscoelastic deformation is only 9%. Therefore, in the analysis of the stiffness of the material the viscoelastic response is neglected.

To determine stiffness properties of the material the loading curve was fitted to a function of the type [17]

$$P = 26.43\, H\, (h-h_0)^n + b \tag{2}$$

where P is the load, h is the displacement, H is the hardness of the material under study and n is a constant; h_0 and b represent the zero correction for the vertical displacement and the load axis, respectively. The hardness is defined as $H=P/F_V$, where $F_V=26.43h_c^2$ is the true contact area for the Vickers indenter and $h_c=h-h_0$ is the corrected indentation depth. The projected contact area for the Vickers indenter with an apical angle 136^0 is $F_V'=F_V \cos 22^0=24.5h_c^2$. The zero correction is necessary to avoid a source of error when manipulating P vs. h data. Thus, the curve fitting on the loading curve is necessary to determine the origin in the load and displacement axis.

3. FINITE ELEMENT SOLUTION

In the present investigation we have used the finite element program ANSYS [10] for the modelling of indentation tests of the polymers. An axisymmetric problem of elasticity with a rigid indenter must be solved. A finite element modelling was performed by using a 1600 eight-node axisymmetric finite elements for the solid and 19 contact elements at the interface between the indenter and the solid. The indenter is represented as a perfectly rigid body. For this mesh there are 9760 degrees of freedom of the finite element problem. A friction contact was modelled by the Coulomb's friction law with a friction coefficient μ=0.2. In the present finite element solution the indenter was modelled as a cone with an apical angle of 136°. Finite element analysis was performed with the given indentation depth and load was calculated as a sum of the vertical nodal forces at the contact surface. For different values of the indentation depth the corresponding load levels were calculated. Let us assume for the numerical experiment that Young's modulus E=3500 MPa and Poisson's ratio ν=0.35. The results of the finite element analysis for ten different indentation depths are presented in Table 1.

It is assumed that the total load P as function of the indentation depth h and elastic parameters of the material can be written in the following empirical form

$$P(h) = f_1(E, \nu; a_i) f_2(h) \tag{3}$$

where E is Young's modulus, ν is Poisson's ratio and a_i are empirical coefficients. The form of the first function $f_1(E, \nu; a_i)$ can be determined from the finite element solution. The second empirical function $f_2(h)$ can be determined by different considerations. From dimensional considerations, one can assume that the average contact pressure must be constant with increasing load and that the function is of the type: $f_2(h) = h^2$. From the approximation of the

loading curves values for the exponent, n, different from 2 can be obtained, i.e. $f_2(h) = h^n$. The function f_1 for the conical indenter is assumed to be of the form

$$f_1(E, \nu; a_0) = \frac{E}{(1-\nu^2)} a_0 = E^* a_0 \tag{4}$$

where E^* is the so-called plane strain elastic modulus. The form of function f_1 is selected from similarity considerations with the analytical solution for the conical punch without friction (see Sneddon [18]). Substituting eq. (4) into (3), and taking into account that exponent n is determined from the experimental loading curve, the total load P can be expressed as follows

$$P(h; a_0) = E^* a_0 h^n \tag{5}$$

From the approximation of the experimental loading curves it was obtained that n=2 for amorphous and crystalline PET and PVF_2, and that n=1.8 for copolymer PVF_2/F_3E 40/60 and for PE.

It should be noted that from the indentation test it is impossible to identify the Poisson's ratio. Therefore, the elastic property to be identified for the polymers from the indentation tests is the plane strain elastic modulus E^*. For identification of the unknown empirical parameter a_0, the least square method is used and minimisation of the following function is performed:

$$\Phi(a_0) = \sum_i \left[\frac{P_i - P(h_i; a_0)}{P_i} \right]^2 \Rightarrow \min \tag{6}$$

where P_i, h_i are data points of numerical experiments (see Table 1), with a number of experiments i=10. In the expression (6) $P(h_i; a_0)$ is defined by the eq. (5) with the fixed value of the exponent n, which is obtained from the data of the physical experiment. Minimisation of the expression (6) was performed by using an algorithm of non-linear programming developed in [19]. The following coefficients for the expression (5) with different values of the exponent n were obtained:

$$P(h) = 1.67 E^* h^2 \tag{7}$$

$$P(h) = 1.78 E^* h^{1.8} \tag{8}$$

Since the finite element modelling was performed with the conical indenter and experiments were performed with the Vickers indenter, the results must be corrected. There are differences between the projected area of the Vickers and the conical indenter. The theoretical ratio is $k=F_V'/F_C'= 4/\pi=1.27$, where $F_V'=24.5h^2$ is the projected contact area of the Vickers indenter and $F_C'=19.24h^2$ is the projected contact area of the conical indenter. The coefficient k can be used to correct the elastic stiffness, since there exists a linear relationship between the load and stiffness. Therefore, the expressions for the load (7) and (8) must be divided by the coefficient k and the corrected formulae are given by:

$$P(h) = 1.31E^*h^2 \tag{9}$$

$$P(h) = 1.40E^*h^{1.8} \tag{10}$$

These formulae were used for identification of the plane strain elastic modulus E^* from the loading curve.

4. CALCULATION OF THE ELASTIC PROPERTIES

Two methods for identification of the elastic properties are used. In this study the P vs. h data in loading and in unloading were employed (see Figs. 2a-e).

4.1 Unloading curve (square punch)

The first method is based on data reduction from the unloading curve. The elastic part of indentation depth h_e is separated by using expression (1) for each load level at the unloading curve

$$h_e(P) = h(P) - (h_p + h_v) \tag{11}$$

For data reduction a formula obtained from the solution of a square punch indentation in elastic half space is used. The slope dP/dh_e is related to the elastic parameters as [6]

$$E^* = \frac{E}{1-\nu^2} = \frac{1}{1.142\sqrt{F'}}\frac{dP}{dh_e} \tag{12}$$

Here $F' = F_V' = 4\,\mathrm{tg}^2\,68^0 h^2 = 24.5h^2$ is the true projected area at the end of the loading cycle (maximum applied force at the indenter). Expression (12) can now be expressed as:

$$E^* = \frac{E}{1-\nu^2} = \frac{1}{1.142\ h\ 2\,\mathrm{tg}\,68^0}\frac{dP}{dh_e} \tag{13}$$

In this case h is the total indentation depth at the maximum applied load at the beginning of unloading (see Fig. 2a-e).

The stiffness dP/dh_e is calculated from the initial part of the unloading P-h curve. The unloading curve is approximated by the function

$$P = A_1 h_e^n \tag{14}$$

or in logarithmic co-ordinates

$$\lg P = n \lg h_e + \lg A_1 \tag{15}$$

The curve fit for amorphous PET is presented in Fig. 4. The approximation in this case gives the expression $\lg P = 1.96\ \lg h_e + 0.43$. The value for the exponent (1.96) is close to 2. With known coefficients A_1 and n, the derivative dP/dh_e of the function (14) can be calculated. Using expression (13) for each experiment, the plane strain elastic modulus is calculated.

4.2 Loading curve

The second method of identification of the elastic properties is based on data reduction from the loading curve. The loading curves (see Fig. 2a-e) are approximated by the empirical functions

$$P(h;a_1) = a_1 h^2, \quad P(h;a_2) = a_2 h^{1.8} \tag{16}$$

By the least square method the value of coefficient a_1 or a_2 is obtained. The expressions (16) obtained by the approximation of the experimental loading curves must be equal to the expressions (9) and (10) obtained by the numerical analysis. From comparison of the expressions (9), (10) and (16) the plane strain elastic modulus can be calculated:

$$E^* = a_1 / 1.31, \quad E^* = a_2 / 1.40 \tag{17}$$

These empirical formulae can be used to determine the elastic properties of the material from the loading curve in the case, when the experimental loading curve is approximated with the exponent n=2 or with n=1.8.

5. RESULTS AND DISCUSSION

Calculations for all five polymers were carried out from unloading and loading curves. From the approximation of unloading curves it was observed that in all cases the exponent n is close to 2. For n=2 the function of the unloading curve P=$P(h_e^2)$ in the P- h_e^2 scale must be linear for the true value of the exponent. Fig. 5 illustrates typical experimental data of unloading curves for different polymers - amorphous PET (PETA), PVF_2 and PE. By comparing the unloading curves for these polymers, it is seen that the elastic stiffness for amorphous PET is higher than for PVF_2, and that the stiffness of PE is higher than that for amorphous PET.

From the approximation of the loading curves it is observed that for amorphous and semi-crystalline PET and PVF_2 the exponent n is close to 2. Fig. 6 shows the typical experimental data for amorphous PET, semi-crystalline PET and PVF_2. Comparison of the loading curves

indicates that the elastoplastic stiffness of semi-crystalline PET is higher than for amorphous PET and than for PVF_2. For high pressure crystallized PE and for $P(VF_2/F_3E)$ 60/40 the exponent n is close to 1.8. The smaller value of the exponent for these polymers is due to the significant plastic deformation involved (see Figs. 2d and 2e). Therefore, in the identification of the elastic modulus from the loading curves it is assumed that n=2 for the amorphous PET, semi-crystalline PET and PVF_2, and that n=1.8 for PE and $P(VF_2/F_3E)$ 60/40. Results of the calculations are presented in Table 2. It should be noted that the slope of the unloading curves was calculated for each experiment, and, therefore, for each unloading curve the exponent n according to eq. (15) is different, but close to 2. Calculations of the elastic modulus from the loading curves for the given polymer were performed with the same exponent for all experiments.

From the analysis of results presented in the Table 2 it is seen that both methods (loading and unloading curves) give about the same values of elastic modulus. The only exception is PE, where the elastic modulus obtained from the loading curve is about 20% lower than the modulus obtained by the loading curve. This difference can be explained since high pressure crystallized PE exibits a rather high elastic modulus [16]. In addition for PE there is a significant plastic contribution to the total indentation depth (see Fig. 2e). Thus, in this case the elastic properties must be identified from the full elastoplastic finite element analysis of the material in loading.

It is of interest to compare the results obtained in the present investigation with other results from the literature. Ion et. al [20] calculated from the microhardness test the elastic modulus E for amorphous PET by using the unloading curve, the formula for the cylindrical punch and lower values of P. The referred values of elastic properties in [20] were: E=3 GPa, ν=0.5 and E^*=4 GPa. The value of E^* is about 20% higher than the elastic modulus obtained in the present paper. However, if instead of using the total indentation depth, h, we use the plastic depth, as proposed by Doerner and Nix [21], then we would obtain the E^* value about 10% higher.

According to Ward and Hadley [22] the value of the elastic modulus E for amorphous PET is about 2 GPa, which was obtained by the experiment with cyclic loading of the material [23]. In [22] the values of Poisson's ratio for PET range from ν=0.36 to ν=0.44. Thus, with ν=0.44

the plane strain elastic modulus obtained from the vibration test [23] is E^*=2.5 GPa, which is about 20% lower than modulus obtained in the present paper.

6. CONCLUSIONS

The proposed numerical-experimental method of identification of elastic properties from the loading curve of the microhardness test of polymers gives similar values of elastic modulus as the calculations from the unloading curve by using the known formula for the square punch. A difference between the values of elastic modulus E^* calculated by the loading and unloading curves was observed in the case of polyethylene due to the high elastic modulus and high level of plastic deformation for this material. In this case the full elastoplastic finite element analysis of the Vickers hardness test must be performed to obtain the behaviour of the material under the indenter upon loading.

ACKNOWLEDGEMENTS

The method of identification of elastic properties of polymers from microhardness tests was developed during the visit of the first author to the Institute of Structure of Matter, Madrid, sponsored by the TEMPUS project JEP 06154-94. The authors would like to thank the project co-ordinator Prof. Dr.-Ing. A. K. Bledzki (University of Kassel) for the opportunity to perform successfully the present study. Thanks are also due to DGICYT, Spain (Grant PB94-0049) for the generous support of this investigation.

REFERENCES

1. H. Sol, J. De Visscher, and W. P. De Wilde, in *Computational Methods and Experimental Measurements VI, Vol. 2: Stress Analysis*, edited by C.A. Brebbia and G.M. Carlomagno, Elsevier Applied Science, London - New York, 1993; pp. 131-142.
2. H. Sol, Identification of anisotropic plate rigidities using free vibration data, PhD thesis, Free University of Brussels (VUB), 1986.
3. L. Bolognini, F. Riccio and F. Bettianli, in *Computational Methods and Experimental Measurements VI, Vol. 2: Stress Analysis*, edited by C.A. Brebbia and G.M. Carlomagno, Elsevier Applied Science, London - New York, 1993; pp. 337-352.
4. C. M. Mota Soares, M. Moreira De Freitas and A. L. Araújo, *Composite Structures*, **25,** (1993), 277.
5. K. L. Johnson, Contact mechanics, Cambridge University Press, Cambridge, 1985.
6. R. B. King, *Int. J. Solid Structures*, **23** (12), (1987), 1657.
7. R. Hill, B. Storåkers and A. B. Zdunek, *Proc. R. Soc. Lond.* **A423,** (1989), 301.
8. A. K. Bhattacharya and W. D. Nix, *Int. J. Solids Structures*, **24**, (1988), 881.
9. A. E. Giannakopoulos, P.-L. Larsson and R. Vestergaard, *Int. J. Solids Structures*, **31** (19), (1994), 2679.
10. ANSYS.Users Manual, Version 5.1, Swanson Analysis System, Inc., 1994.
11. A. K. Bhattacharya and W. D. Nix, *Int. J. Solids and Structures*, **24** (12), (1988), 1287.
12. F. J. Baltá Calleja, *Trends in Polym. Sci.* **2** (12), (1994), 419.
13. C. Santa Cruz, F. J. Balta Calleja, H. G. Zachmann, N. Stribeck, and T. Asano, *J. Polym. Sci: Part B: Polym. Phys.*, **29**, (1991), 819.

14. F. J. Balta Calleja, C. Santa Cruz, A. Gonzalez Arche and E. Lopez Cabaros, *J. Mater. Sci.*, **27**, (1992), 2124.

15. A. J. Lovinger, in *Developments in crystalline polymers, J. Appl. Sci., vol. 1, ch. 5*, edited by D. C. Bassett, Applied Science Publishers, London, 1982; pp. 195-273.

16. D. C. Bassett and D. R. Carder, *Phil. Magazine*, **28** (3), (1973), 535.

17. F. J. Balta Calleja, D. R. Rueda, R. S. Porter and W. T. Mead, *J. Mater. Sci.*, **15**, (1980), 765.

18. I. N. Sneddon, *Int. J. Engng Sci.*, **3**, (1965), 47.

19. R. Rikards, in *Optimal Design with Advanced Materials, Proceedings of the IUTAM Symposium, Lungby, Denmark, 18 - 20 August, 1992*, edited by P. Pedersen, Elsevier Science Publishers, Amsterdam, 1993; pp. 149-161.

20. R. H. Ion, H. M. Pollock and C. Roques-Carmes, *J. Mater. Sci.*, **25**, (1990), 1444.

21. M. F. Doerner, and W. D. Nix, *J. Mater. Res.*, **1** (4), (1986), 601.

22. I. M. Ward and D. W. Hadley, *An Introduction to the mechanical properties of solid polymers*, John Wiley and Sons, Chichester, 1993.

23. A. B. Thomson and D. W. Woods, *Trans. Faraday Soc.*, **52**, (1956), 1383.

TABLES

Table 1 Results of the finite element solution by program ANSYS for the conical indenter.

Number of numerical exper.	Indentation depth h μm	Load P gf
1	0.5	0.173
2	1	0.634
3	1.5	1.479
4	2	2.651
5	2.5	4.106
6	3	5.959
7	3.5	8.056
8	4	10.606
9	4.5	13.389
10	5	16.629

Table 2 Plane strain elastic modulus E^* (in GPa) for different polymers calculated from unloading (eq. (13) for the square punch) and loading (eq. (17)) curves.

Polymer	Number of experi-ments	Method of identification		
		Unloading curve	Loading curve	
		E^*	E^*	n
amorphous PET	18	3.22	3.06	2
semi-crystalline PET	10	3.96	4.17	2
PVF_2	10	2.77	2.87	2
$P(VF_2/F_3E)$ 60/40	10	1.69	1.80	1.8
PE	10	4.31	3.38	1.8

CAPTIONS TO FIGURES

Fig. 1: Typical variation of load versus time in the performed experiments

Fig. 2: Plot of load versus indentation depth for polymers investigated:
a)-amorphous PET; b)-semi-crystalline PET; c)-PVF_2;
d)-$P(VF_2/F_3E)$ 60/40; e)-PE

Fig. 3: Plot of indentation depth versus time for the sample of amorphous PET

Fig. 4: Curve fit for initial part of the unloading curve for amorphous PET

Fig. 5: Plot P against h_e^2 for the unloading cycle of the various polymers: 1-PE , 2-amorphous PET, 3-PVF_2

Fig. 6: Plot P against h^2 for the loading cycle of the various polymers:
1- semi-crystalline PET, 2-amorphous PET, 3-PVF_2

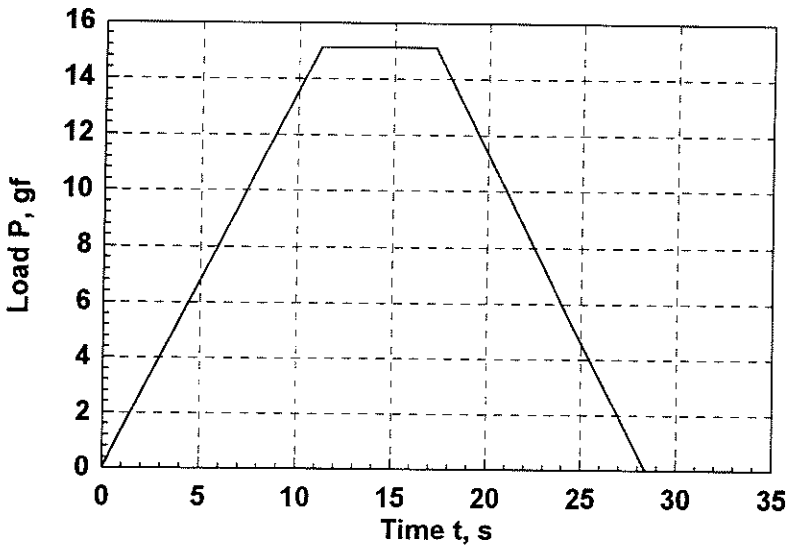

Fig. 1: (R. Rikards et.al).

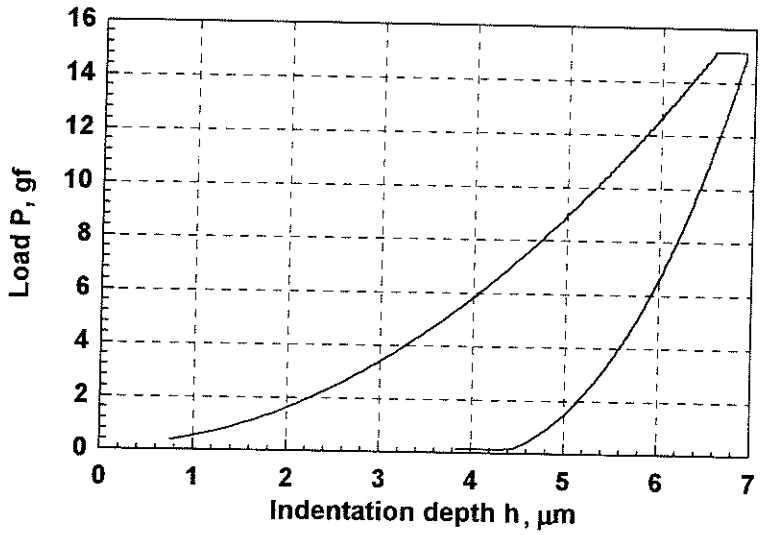

Fig. 2a: (R. Rikards et. al).

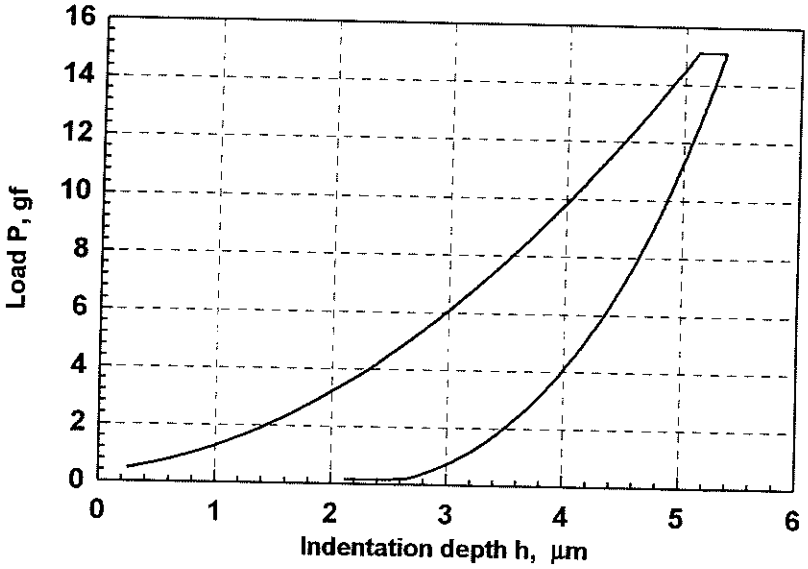

Fig. 2b: (R. Rikards et. al).

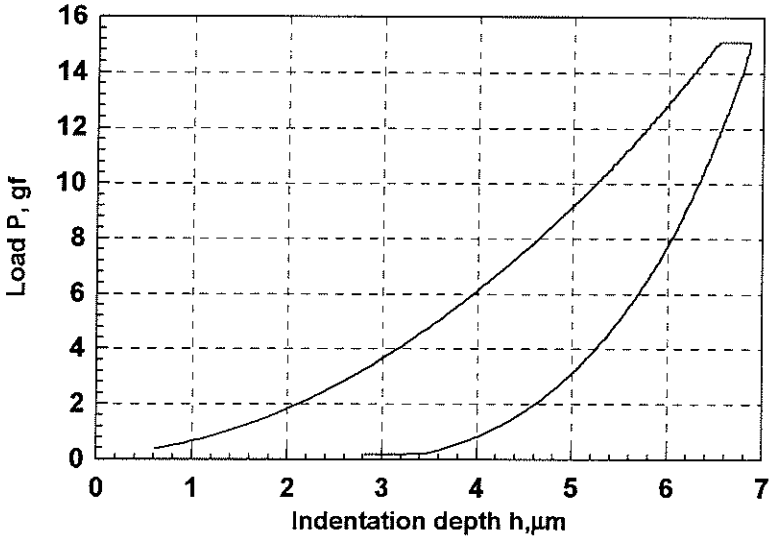

Fig. 2c: (R. Rikards et. al).

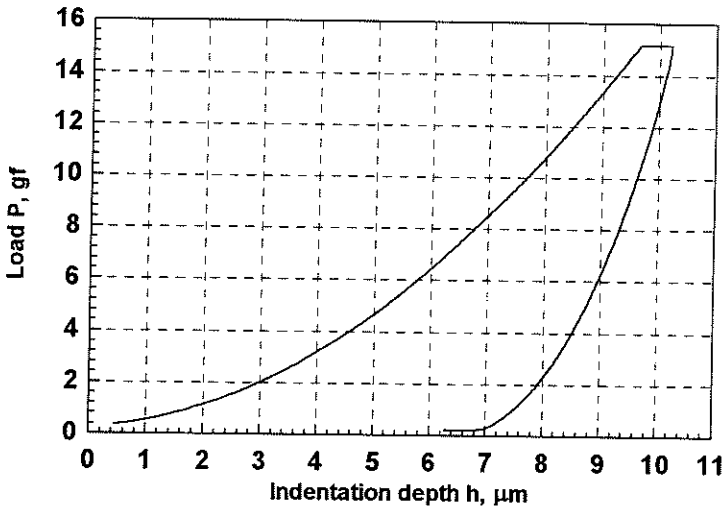

Fig. 2d: (R. Rikards et.al).

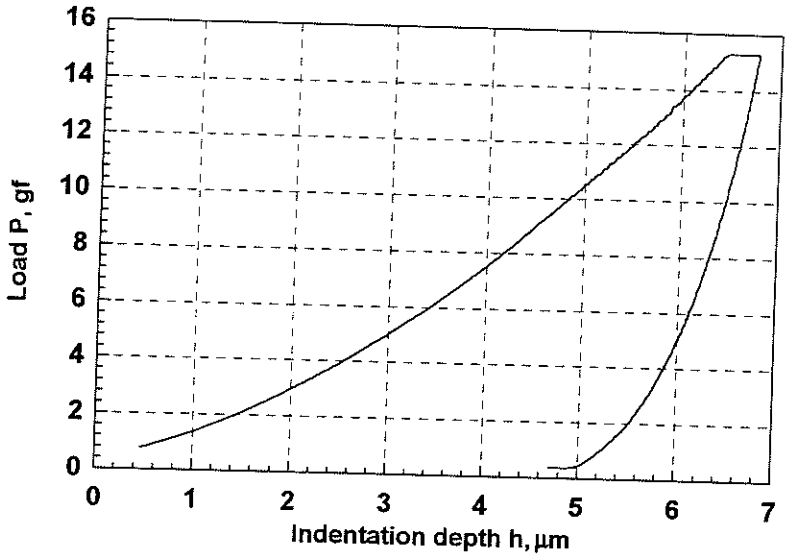

Fig. 2e: (R. Rikards et. al).

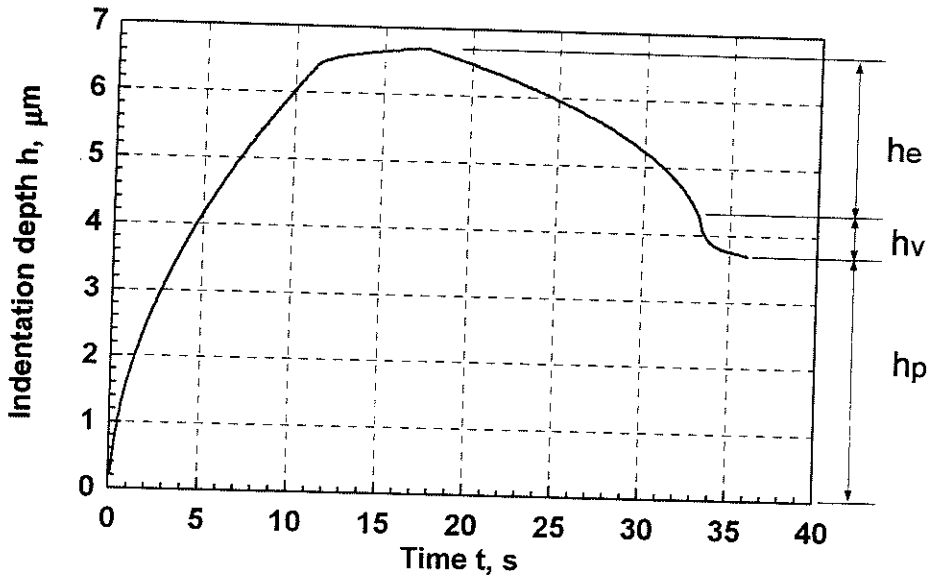

Fig. 3: (R. Rikards et. al.).

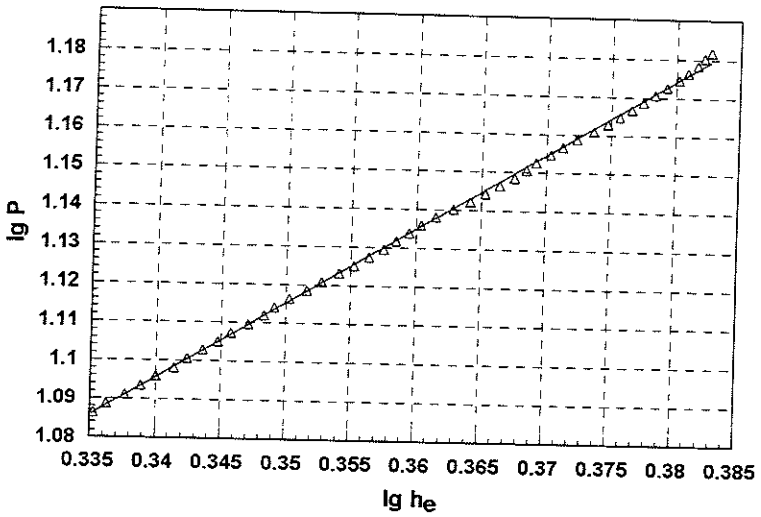

Fig. 4: (R. Rikards et. al).

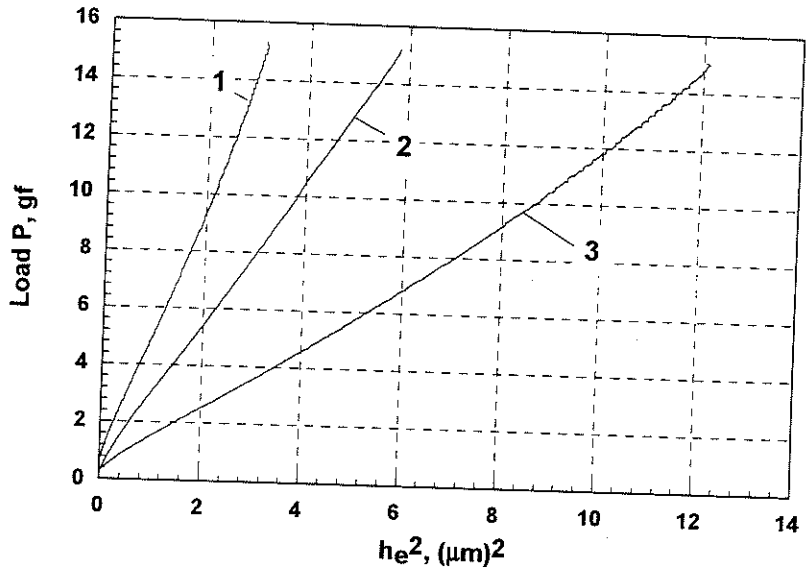

Fig. 5: (R. Rikards et.al).

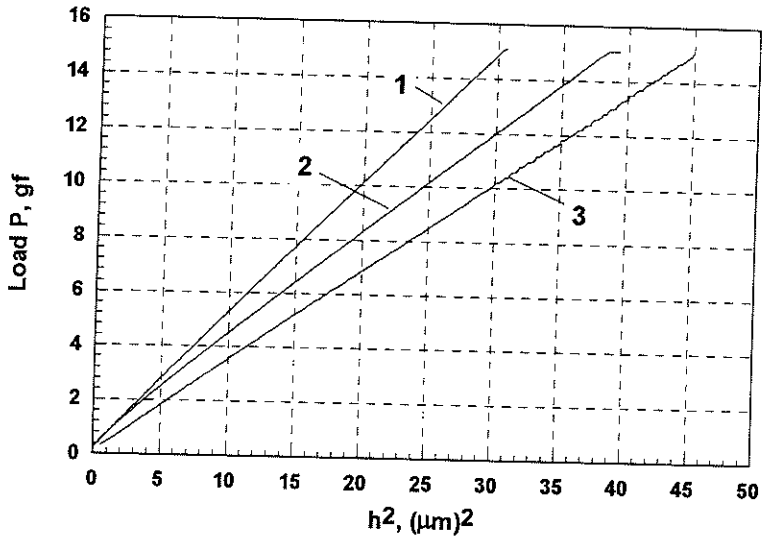

Fig. 6: (R. Rikards et. al).